3D-Self-Assemblage and Self-Organization on Natural Colloidal Microinclusions in Mineral Sediments

A.P. Kuzmenko[1], Chan Nyein Aung[1], V.V. Rodionov[1], M.B. Dobromyslov[2]

[1] *South-West State University, 94, 50 Let Oktyabrya Str., 305040 Kursk, Russia*
[2] *Pacific National University, 136, Tikhookeanskaya Str., 680035 Khabarovsk, Russia*

The results of micro- and nanoscale research of fractal structure sediments from mineral water received by the drop method are given. Qualitative analysis of the underlying physical phenomena, allowed us to establish the conditions of their 3D-fractalization that consider the size of colloidal nanoparticles, its location and height from the drop center : $r_{min} = R_{max} = h_{max}$ and $r_{max} = R_{min} = h_{min}$. It is shown that the main contribution to 3D fractalization is due to surface tension forces and the Coulomb force interaction.

Keywords: Self-assemblage, Self-organization, Fractal structure, Colloidal micro and nanoinclusions, Surface tension, Coulomb force interaction.

1. INTRODUCTION

Changeover to the electronic elemental base with transistor elements of a nano-domain size (~ 10 nm) [1, 2] indicates that traditional technological approaches are faced with the problem that is due to fundamental physical limits, making progress in nanoelectronics critically difficult. This is dictated in many ways by the fact that the changeover to nano-domain is accompanied by a manifestation of new physico-chemical effects [3], in particular, self- organization and self-assemblage, on practical use of which development engineers of both electronics and new nanostructured materials place great hopes.

In this connection , natural drop-like entities that contain colloidal micro-inclusions with particle radius (R) whose total energy (E) is determined in this way: $E = \alpha R^3 + \beta R^2 + \gamma R$, where contributions of volume energy $- \alpha$, surface energy $- \beta$ and surface tension $- \gamma$ are included, present an appropriate model for studying regularities in space self-organization and self-assemblage. In [4] with 2D-cell automate a computer planar model was examined of self-assemblage and self-organization of cluster nanodendritic formations, as components of noncovalent synthesis, as a result of adhesion between molecules and ensembles with consideration for the density distribution of diffusing particles. However, planar problems were sold only. Formation of columnar semiconducting polymeric nanostructures that originate in spin casting with consideration for the effect of substrate, solvent, concentration and external electric field applied was investigated in [5]. Synthesis and study of self-assembled 3D droplet colloidal microstructures formed at a superhydrophobic surface that has nucleating structural elements of colloidal sizes as functions of evaporation conditions, number of particles and their size are considered in [6]. The workers in [7], as applied to binary systems from metals, proposed an analytical model of cluster self-organization via voluminous crystallization in a supercooled state that considers their kinetic variations, nonlinearity, and processes of their generation as being non-equilibrium. Those formations are assigned

sets of eigen-frequencies. Parametric or resonant excitation of these frequencies makes it possible, according to [7], control the crystallization of cluster binary systems. The results of investigation with fractal structures (FSs) from heterogeneous and heterophase systems of natural origin are provided in [8, 9]. Those structures were obtained by the drop method when hydrodynamic streams and gravitational effects are small i.e. $L < (\sigma / \rho g)^{1/2} \sim 3$ nm for water, and capillary forces (dependent on surface forces σ), adsorption, and interphase forces that are dependent on the density of interacting systems, are major contributors to the processes of self-organization and self-assemblage.

The data obtained on 3D-fractalization in distribution of chemical elements and compounds that appear as a result of mineral waters (MWs) evaporation presenting ideal natural colloidal solutions, in our view, add to the knowledge about self-organization and self-assemblage in such systems and are of great importance for the developments in nanomaterial science and electronics.

2. EXPERIMENTAL PROCEDURES

Sediments of MWs from mineral springs of Northern Caucasus and Kursk region (Russia) have been studied. These MWs are characterized by a diversity of cation and anion colloidal formations from which at normal conditions (NCs) dendritic structures are formed after precipitation by the drop method. The features of FSs have been studied with the help of atomic-force microscope (AFM) (SmartSPM AIST NT,Russia), scanning electron microscope (SEM) – (JSM 6610-LV, JEOL, Japan), digital holographic microscope (Lynceetec, Switzerland). The elemental composition of FSs and their distribution through thickness were analyzed by energy dispersive analysis (EDA) – (EDX Oxford Instruments, Great Britain). Chemical structure was determined by IR-Fourier spectroscopy (NicoletiS50, Thermo Fisher Scientific, USA).

Self-organized structure formations formed by the droplet method feature indisputable advantages, namely,

simplicity and range of applicability. To form FSs substrates from glass, single crystal silicon and aluminum were used. It turned out that the most contrast SEM-images were formed at a silicon substrate. Typical SEM-images of such structures from MWs of Borjomi, Essentuki (Caucasus) – 4 and 17 are given in Fig. 1 a-c. Similar structures were formed from MWs of Kursk region.
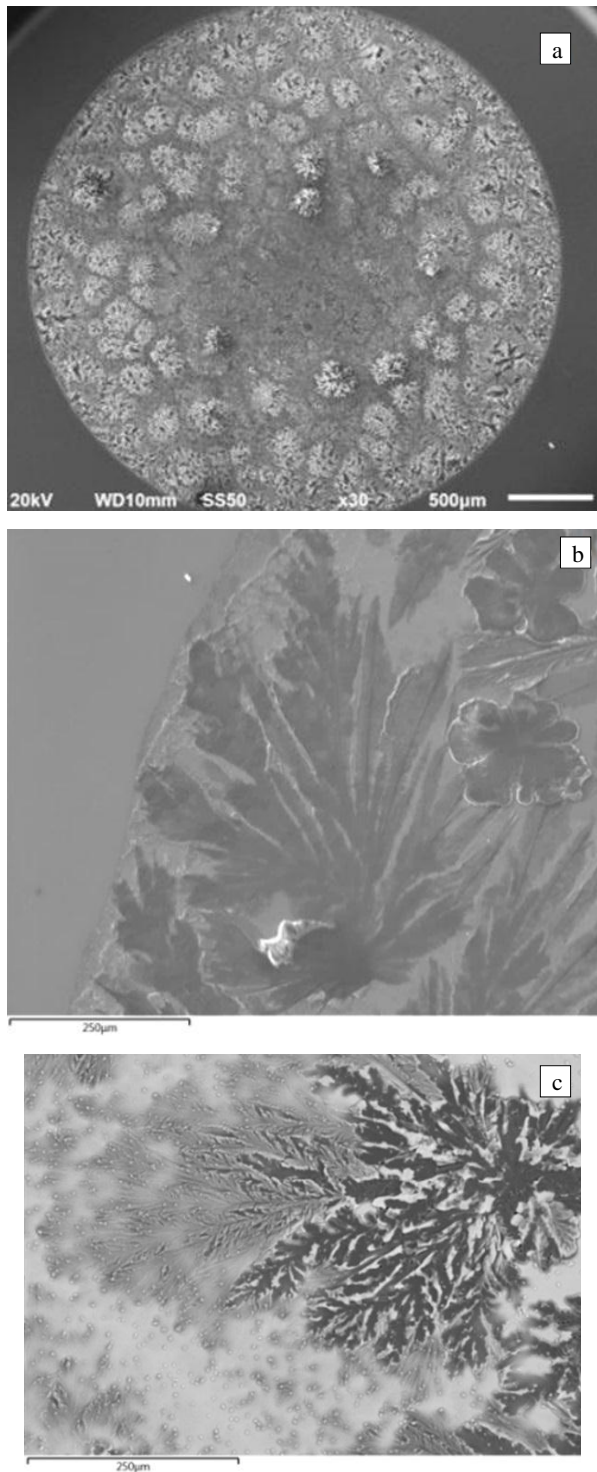

Fig. 1 – SEM-images of MW sediments at a silicon substrate: a – ring-formation from Borjomi FSs, b and c – fragments of FSs Essentuki 4 and 17, respectively

Table 1 – Elemental analysis of FSs in sediments of different MWs with the evaluation of the degree of each element

Minerals		Elements						
		C	O	Na	S	Cl	Ca	Mg
Essentuki 4	At fractal	10	48	20	–		–	–
	At. Wt. %	19	47	27	–	6	–	1
Essentuki 17	At fractal	17	59	75	–			
	At. Wt. %	20	41	26		12		
Borjomi	At fractal	10	41	27	–			
	At. Wt. %	22	48	23		5	1	
Spring 1 Kursk	At fractal	–	11	6	69		32	–
	At. Wt. %	–	43	7	3		9	3
Spring 2 Kursk	At fractal	–	27	11	63		42	
	At. Wt. %	–	48	7	4		9	3

The EDA data of chemical element distribution that form FSs are given in Fig. 2 a-b in which, as an example, an individual fragment sediment of Essentuki – 4 is shown in Fig. 1 b. Comparison of SEM-images of many-layered EDA (see Fig. 2 a) with images of their distributions for Na and Cl indicates a coincidence both in terms of the general configuration and in details of individual elements: Na, O, and C. The distribution of these elements in the central part of FSs is characterized by uniformity. At the same time, the elemental distribution for Na occurs, which repeats only external contour of FSs. This feature is typical of all other sediments studied, in which chlorides and carbonates are well representative. Fig. 2 c shows SEM-images of both the whole studied FS (transverse size 211 μm) and the detailed image of its edge fragment with the size of 8.6 μm (insert). It should be noted that the elemental analysis data indicate the absence of Cl just in this part. Image in Fig. 2c on morphological structure has whiskers (crystals) [10].
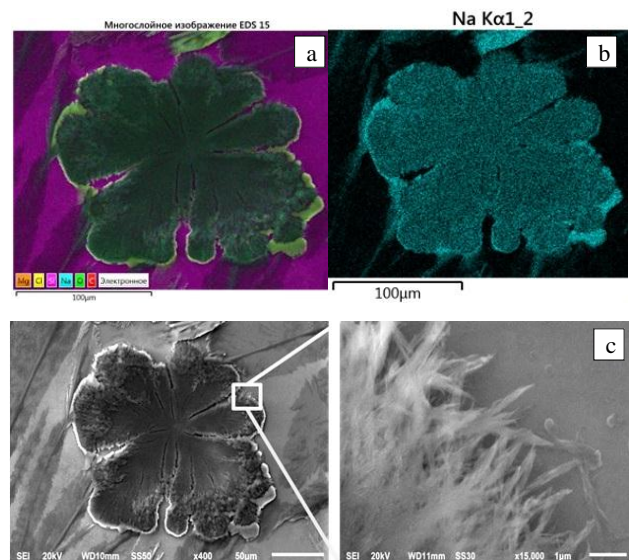

Fig. 2 – Elemental distribution in FS on MWs sediments Essentuki – 4: a – general view of elements (Mg, Cl, Si, Na, O, C), b – for Na, c – SEM-image of FS and its enlarged by 15×10^3 times edge fragment

Table 2 – Chemical composition of FS according to EDA data dependent on the accelerating voltage value, kV. The denominator shows predicted radius of electron penetration, μm

Voltage, kV	Atomic weight, % / predicted penetration radius, μm				
	C	O	Na	Mg	Cl
2	46.3/0.02	26/59.7	25.9/0.06	1.9/0.04	– /0.02
3	26/0.04	36/117.5	37/0.12	1.5/0.07	– /0.04
5	21.7/0.1	34.6/276	29.3/0.28	0.8/0.16	13.6/0.09
10	20.5/0.33	41.4/878	28.1/0.9	0.6/0.52	6.4/0.29
20	21.8/1.04	45.8/2794	26.2/2.87	0.6/1.66	5.6/0.9

EDA made it possible, at various accelerating voltages (2, 4, 5, 10, and 20 kV) when the penetration depth of the electron beam is varied, to determine the content of chemical elements at different levels from surface in all FS studied (Table 2). The variation in content of individual elements with depth can be indicative of their 3D distribution in FS sediments. For example, content of C and Mg continues to be constant starting from 5 kV, whereas at this voltage Cl only begins to be detected, which is clear proof that Cl sets in the low part of FS.

Analysis of images of FS formations obtained with digital holographic microscope also points to their tridimensionality. Given in Fig. 3 a is a reversed image of 3D-image of such structure and its profile along one brunch of FS: from the center to the edge with height difference within the range from – 50 to – 370 nm. As is seen from Fig. 3 b the height variation of FS is of stepwise character. The heights determined from the figure at different levels of FS with respect to the substrate are given in Table 3. The FS thickness from the top level (– 370 nm) monotonically decreases taking on values 303, 285, 165, and 137 nm. This series of values is approximated with the expression $h = -0.12r^2 + 1.09r - 0.1$, where r is the distance from the FS center. Tridimensionality of FS is also supported by the data of SEM-images (see Fig. 3 c) from which it follows that the maximum height difference value of the sediment is on the order of 40 μm.
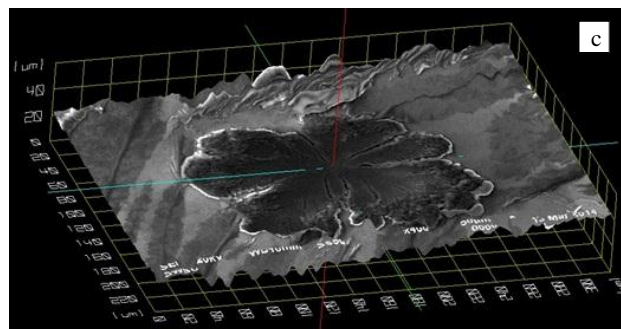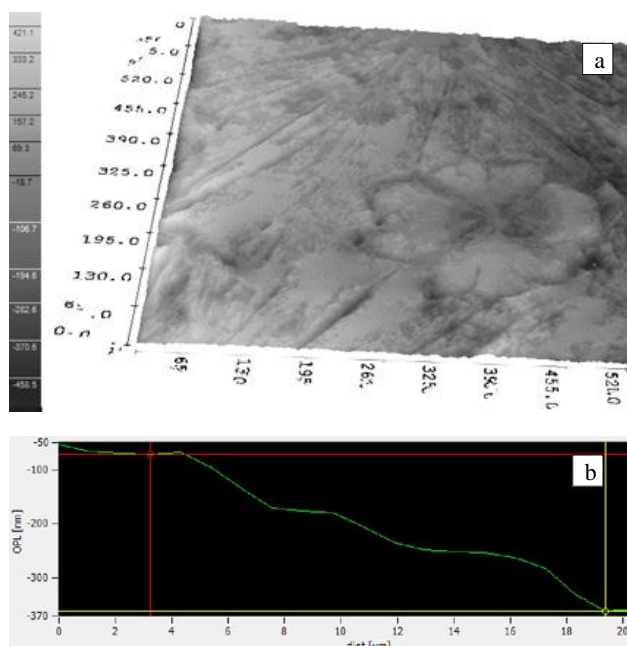

Fig. 3 – Image of one fractal from the sediment of Essentuki-4: a – 3D-image, b – it's profile, c – 3D-SEM-image

Table 3 – Variation of FS height above the level of the silicon substrate (see Fig. 3 b)

Kind of mineral water	The height and number of levels above the substrate fractal Si (*h*), μm			
	0-1	0-2	0-3	0-4
Essentuki-4	0.135	0.44	0.725	0.89
Essentuki-17	1.3	2.2	2.8	3.2
Borzhomy	1.2	2.2	2.8	3

As is seen from Fig. 3 b to this distribution of compounds of Cl and Na (specifically, sodium bicarbonate) there corresponds the low step (– 70 nm in the reversed image). This fact is in reasonably good accord with SEM-data (see Fig. 2 c, insert) according to which compounds of $NAHCO_3$-type are detected just at the edges of FS. It can be proposed that the following steps correspond to the chemical compounds with lower molecular mass that contain Mg, Na, etc., that are the components of all studied sediments of MWs.
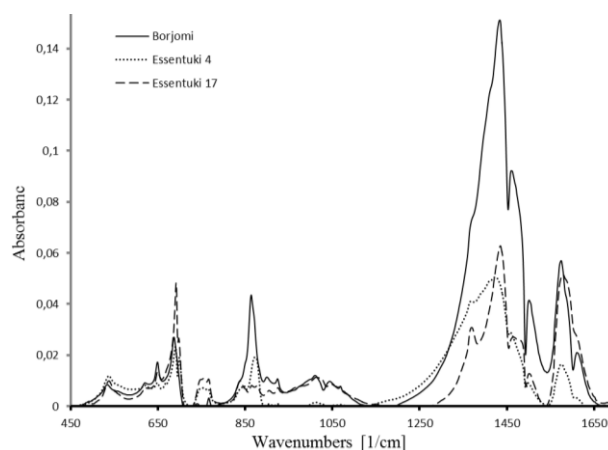
Fig. 4 – IR-spectra of FS in MW sediments

For all MWs in the fundamental range of the IR-absorption spectrum absorption at lines 3397 and 1640 cm^{-1} occurred. For the determination of chemical structures that form FS because of the material under study was small in both size and amount only IR-Fourier spectroscopy was found applicable. IR analysis spectra obtained for MW sediments with FS beginning from the edge of the middle range 450 cm^{-1} and up to 1700 cm^{-1} are shown in Fig. 4, and appearing absorption lines and their identification are given in Table 4.

Table 4 – IR spectra of MW sediments

Compound	Absorption lines (cm^{-1})		
	Borzhomy	Essentuki-4	Essentuki-17
H_2O_4S	1610		
$H_3BO_3^{3-}$, Cl^-	1574	1575	1578
	1500	1498	1501
	1460	1457	1466
	1434		1435
		1424	
NO_3^-		1367	1370
BO_3^{3-}, SiO_4^{4-}	1068		
	1044		1047
	1010		1014
	924		925
			905
	899		
SO_4^{2-}		872	877
CO_3^{2-}	863		865
Cl^-		847	
CO_3^{2-}, NO_3^-			838
BO_3^{3-}, SiO_4^{4-}		765	766
		754	754
		700	
		690	691
	648	648	649
SO_4^{2-}	620	620	620
		595	
SiO_4^{4-}, SO_4^{2-}	534	538	538

3. RESULTS AND DISCUSSION

It should be stressed that FSs were formed from compounds and trace elements that are constituents of MWs in a cation or anion form (as carbonate, sulfate, and other chemical compounds – Table 4).

EDA conducted at different accelerating voltages (see Table 2) makes it possible to calculate radii of penetration area for the electron using empirical dependence that follows from the Bethe equation at Kanaya-Okayama approximation: $H = 0.276\, AE_0^{1.67} / (Z^{0.88}\, \rho)$. Here A and Z are atomic weight and number of chemical element, E_0 is the energy of incident electrons $E_0 = eU$, ρ is density. The prediction results are given in Table 2. Numerical analysis of collision trajectories of electrons with atoms of FS studied carried out with a lot of electrons (not less than 100) by the Monte-Carlo method made it possible to determine the size of this interaction area for some compounds. In particular, for sodium bicarbonate (NaHCO$_3$), one major sediment component in MW Essentuki-4, calculated diameter of interaction area and penetration depth at voltages of 3, 5, 10, and 20 kV amounted to 316, 720, 2080, 8800 nm, respectively for the diameter and 240, 446, 1580, 6700 nm – for the depth. Calculated diameter of the interaction area at an accelerating voltage of 20 kV

(8,8 μm) has practically coincided with the size of observed area with filamentary crystal formations characteristic of NaHCO$_3$ – 8.6 μm (see Fig. 2 c, insert). Such structure is typical of NaHCO$_3$ [10]. As was noted, this inference follows from the transverse profile of FS (see Fig. 3 b and Table 2). In this case, the sizes of relevant areas are in good agreement.

Analysis of IR spectra revealed that the spectral resolution of 1 cm^{-1} is enough for studying those micro-objects since absorption lines observed in a MW drop correspond to the following vibrations: along or perpendicular to the c axis – radial vibrations of the II and asymmetric vibrations of the I type, respectively. In [11] according to IR- spectroscopy difference in frequencies of these vibrations (ν_1 and ν_2) are found, respectively by 54 and 35 cm^{-1} in the water layer of about 100 μm thickness. It is noted that ν_1 shifts to the low-frequency domain with increasing thickness of samples studied and ν_2, conversely, shifts to the high-frequency domain. In our case at a typical MW thickness of order 250 μm according to IR-spectroscopy the second type vibrations are excited, for which two scenarios are implemented, namely, as a single connection of a water molecule with a Na cation or as a connection with the cation of two water molecules. In doing so, we also note an increase in the frequency shift between the vibrations (ν_1 and ν_2) in diametrically opposed directions, which supports the applicability of IR spectroscopy for studying colloidal microinclusions as in both water solutions and their sediments.

Using spectra of originating vibration excitations on FSs in MW sediments (Fig. 4) with data base [12] anionic (hydrogen carbonate – HCO$_3^-$, sulfate – SO$_4^{2-}$, chloride – Cl$^-$) and cationic (calcium – Ca^{2+}, magnesium – Mg^{2+}, sodium and potassium – Na$^+$, K$^+$) are identified (see Table 4). Molecular masses of compounds formed from these colloidal microinclusions, in particular, NaHCO$_3$ and sulfates of sodium, potassium, magnesium are equal to 84, 120, 142, 174 g/mol, respectively. According to EDA data for FSs, content of Mg^{2+} and K$^+$ is barely detected and hence their contributions can be neglected. From analysis of IR spectra (see Fig. 4) total intensities (the sum of all lines in IR Fourier spectra) for every colloidal microinclusion for all given chemical compounds are $I_{\Sigma CO_3^-} = 38.5\,\%$, $I_{\Sigma SO_4^{2-}} = 7\%$, $I_{\Sigma BO_3^-} = 6.9\,\%$. It follows from here that the major role at the initial stage of fractal-formation is played by exactly hydrocarbides of NaHCO$_3$ – type and chlorides Ca, Mg, Na, and K that have most molecular mass. In other words, distribution of chemical elements and compounds across the FS height is described by an empirical dependence of the type $H \sim \mu^{-1}$.

Using assumptions proposed by J.K. Maxwell for studying processes in the droplet within diffusion model of solvent evaporation (MW) into the atmosphere. According to them gravitational force, temperature reduction, and auto vibration can be ignored, i.e. the Marangoni effect is not considered. Indeed, in our case for MWs studied evaluations $Mg = L\Delta T(a\eta)^{-1}\, d/dT$ give very small value $Mg \ll 1$ since both surface tension variations as a function of temperature (ΔT) and the droplet diameter (L) are extremely small. And parameters η – dynamical viscosity, a – temperature con-

ductivity of water and σ become dominant in dictating the quantity Mg. This means that in fractalization there are no convection phenomena.

The most important processes, which affect the droplet shape due to the evaporation of colloidal solution, are hydrodynamic streams within the droplet and the interaction between the microinclusions and the substrate. All studied were conducted in the pinning mode along the contact line "water-substrate" i.e. at high wettability of the droplet with the substrate. To analyze the interparticle interactions of microinclusions in the solution and on the substrate we utilize conclusions from [13]. Geometry and material composition (MW and colloidal microinclusions) dictates implementation of the fractalization scenario: water evaporation $\rightarrow$ hydrodynamic stream $\rightarrow$ radial distribution of particles. Ring-like shape of FSs in all MW sediments (see Fig.1 a) supports this scenario.

Radial motions of microinclusions are described by the dissipative dynamics as Langevin's equations modernized by workers in [13]. The existence of anion and cation microinclusions in MWs requires consideration of Coulomb interactions $F_c = q_i q_j / (4\pi\varepsilon\varepsilon_0 r_{ij}^2)$, which critically influences on the dynamics of motion of colloidal particles and their fractalization. In our view, consideration of F_c corresponds as well to experimentally found quadratic dependence of FS height variation for different colloidal microinclusions. The final equation of motion of particles is the following:

$$m\frac{dv_i}{dt} = m\left(\frac{\partial V}{\partial t} + v(\nabla V)\right) -$$
$$-\sum_{i \neq j}^{N} \nabla U(r_{ij}) + F_s(r_s) + F_L(r_L) - 6\pi a\eta(v_i - V) + F_B + F_C$$

This equation includes interaction forces with the substrate – $F_s(r_s) = -nA_s\exp(-ar_s)$ and with interphase boundary "water-air" – $F_L(r_L) = 2\pi Rfn$ for $|r_L| < \{h, L\}$ (only particles within the droplet of height h and diameter L are considered). Here n is an internal unitary normal to the interphase boundary "water-air", f is the effective density of surface energy (per unit area of the contact between a particle and a solvent) of sum of the interaction forces between i-th and j-th particles if part of the potential from the well known model of Derjaguin-Landau-Vervey-Overbik acts as a Debye-Gakkel's function in the form $U(r) = (A / r)\exp(-r / \lambda)$, where λ is the Debye shielding distance for the particle, $A = (Ze \exp(-R / \lambda)^2 / (4\pi\varepsilon\varepsilon_0(1 + R / \lambda)^2)$ is a constant dictated by particle characteristics. Considered also are the Stokes force of the viscous friction, $6\pi R\eta(v_i - V)$, the random force of the Brownian motion of the Gauss form, F_B, and the forces due to droplet volume variation, $m[(\partial V / \partial t) + v(\nabla V)]$.

The given equation of dynamics takes properly into account the role of Coulomb forces, which earlier were considered only in the interaction potential $U(r)$ with consideration for λ. Colloidal microinclusions in MWs studied, as it follows from IR analysis, have the electrical charges that vary in sign and value. For example, there are anionic charges SO_4^{2-}, Cl^-, and also cationic charges Ca^{2+}, Mg^{2+}, Na^+, K^+. The present composition has an additional effect on the processes of radial mo-

tions of colloidal microinclusions, which are accompanied by neutralization of charges and their agglomeration (coagulation). In the most general case the interaction potential of colloidal particles with charges Z_i and Z_j, radii R_i and R_j with distance between them being r, according to [14] is: $U_{ij}(r) = k_B T Z_i Z_j \lambda_{up} k(R_i + R_j - r)[(1 + kR_i)(1 + kR_j)r]^{-1}$. At a first approximation we obtain $U_{ij}(r) \sim k_B T \lambda_{up} k(R_i + R_j - r) / r$, where $k = (8\pi\lambda_B C)^{1/2}$, and $\lambda_B -$ the Bjerrum length, which equals 0.7 nm for H_2O at normal conditions. Extrapolation of dependence $U_{ij}(r)$ at the initial and final sites makes it possible to find characteristic distances: r_{min} and r_{max} from the droplet center that determine the range for the given system from particles with the maximum and minimum radii: $r_{min} = R_{max}$, and $r_{max} = R_{min}$, where the scenario of stable fractal- formation should be implemented.
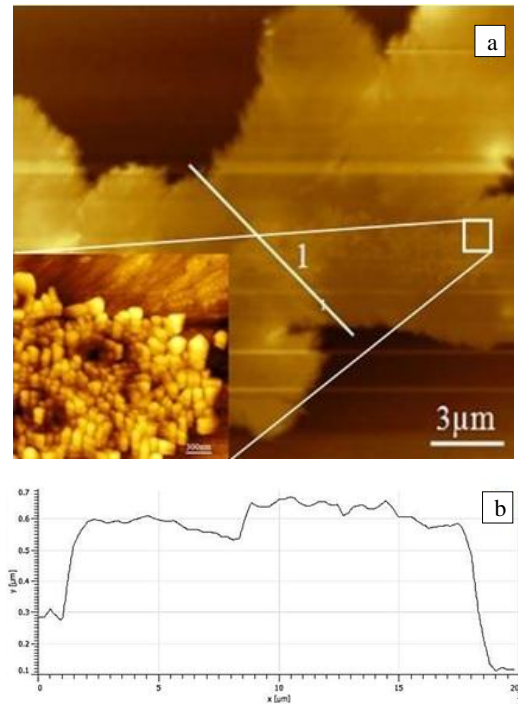
Fig. 5 – a – AFM images of the FS fragment and its part (2×2 μm), b – transverse profile of FS along the line "1"

Under isothermal conditions for heterophase colloidal systems the rate of FS formation essentially depends on quantities R and E. In accordance with Stokes-Einstein's formula $D = k_B T / (6\pi R\eta)$, the value of the diffusion coefficient of particles in a solution is inversely dependent on their size. This means that large particles are not capable of traveling long distances and are obviously the first to precipitate, other things being equal. Of note is the fact that the rate of particle agglomeration is determined by the Fouks formula: $\partial n / \partial t = -8\pi RDn^2 \exp(-E / k_B T)$. Here n is concentration of non-agglomerated particles, D is the diffusion coefficient of particle in a solution, E is the height of energy agglomeration barrier, T is the solution temperature. Virtually, the Fouks formula dictates the rate of particle unification with the FS formation, which is reduced with increase in E, diffusion layer thickness, and also with reduce in the dropt radius. Agglomera-

tion indicates both higher rate of this process for larger particles (radii R_i or R_j), and the existence of differing in height potential barriers (E), which is indirectly supported by a stepwise nature of FS (see Fig. 3 b and Table 3). In doing so, the droplet height is of critical importance. Obviously, as soon as the droplet becomes the size of large particles, their diffusion motion either turns difficult or stops at all, which corresponds to the low limit of the fractalization range. Similarly with further evaporation, when the droplet height reaches the minimum particle size their diffusion translations also become impossible.

Thus, there is reason to believe that 3D fractalization occurs if the following equalities are fulfilled: $r_{\min} = R_{\max} = h_{\max}$ and $r_{\max} = R_{\min} = h_{\min}$. This conclusion is supported by AFM images presented in Fig. 5 a and insert with shown AFM images: of the whole FS fragment in the field 21×21 µm and its part $- 2 \times 2$ µm. Here shown is the profile of AFM image with cross-section of one branch of FS along the line "1". Measuring accuracy across profile cross-section along Z-coordinate

was not greater than 40 pm. The profile of cross-section has three areas differing in height. Two extreme ones are virtually coincide whereas the middle is elevated by nearly 50 nm. It should be noted that this area is formed from nanoparticles the size of 100 nm, as is seen from insert to Fig. 5 a. Here the height differential at different FS components coincided with its measurement (see Fig. 3 b and Table 3) according to which it was determined with an accuracy of order 1 nm, typical of utilized holographic microscope.

4. CONCLUSIONS

The results obtained in nano-scale investigations of self-organization and self-assemblage processes of colloidal microinclusions observed in mineral water sediments, and deduced conditions for their fractalization are of great practical importance for both modeling these phenomena and design, on their basis, of novel nanostructured materials and components, including the field of electronics.

REFERENCES

1. Wei Lu, Ann Marie Sastry, *IEEE T. Semiconduct. M.* **20** No 4, 421 (2007).
2. R.P. Seisyan, *Tech. Phys.* **56** No 8, 1061 (2011).
3. G.B. Sergeyev, *Chem. J. Russ.* **46** No 5, 22 (2002) [In Russian].
4. S.A. Beznosyuk, Ya.V. Lerkh, T.M. Zhukovskaya, *Polzunovsky Vestnic* No 4-1, 143 (2005) [In Russian].
5. Tauc-Quyen Nguyen, Richard Martel, Mark Bushey, et al., *Phys. Chem. Chem. Phys.* **9**, 1515 (2007).
6. A.G. Marin, Hanneke Gelderblom, Arturo Susarrey-Arce, et al., *PANS* **109** No 41, 16455 (2012).
7. F. Mizade, *Tech. Phys.* **51** No 9, 1183 (2006).
8. A.P. Kuzmenko, V.V. Chakov, Chan Nen Aung, *Nauzn. Vedomosti of Belgorod State University. Series: Mathematics. Physics* **154** No 11, 174 (2013) [in Russian].
9. A.P Kuzmenko, V.V. Chakov, Chan Nyein Aung, M.B. Dobromyslov, *J. Nano- Electron. Phys.* **5** No 4, 04019 (2013).
10. A.A. Mohammad, Ali Morsali, *Nanocrystal. – ISBN 978-953-307-199.* 237 (2011).
11. J. Fukuda, K. Shinoda, *Phys. Chem. Mineral.* **35**, 347 (2008).
12. Database of IR spectroscopy: http://sdbs.db.aist.go.jp/sdbs/cgi-bin/direct_frame_top.cgi.
13. L.V. Andreeva, A.V. Koshkin, P.V. Lebedev-Stepanov, A.N. Petrov, M.V. Alfimov, *Colloid. Surface. A: Phys.-Chem. Eng. Aspects* **300**, 300 (2007).
14. E.L. Mirjam, G.C. Christina, Antti-Pekka Hynninen, et al., *Nature* **437**, 235 (2005).